

# Open Cell Conducting Foams for High Synchrotron Radiation Beam Liners

S. Petracca,\* A. Stabile†

*Dipartimento di Ingegneria, Universita' del Sannio,  
Palazzo Dell'Aquila Bosco Lucarelli,  
Corso Garibaldi, 107 - 82100, Benevento, Italy*

## Abstract

The possible use of open-cell conductive foams in high synchrotron radiation particle accelerator beam liners is considered. Available materials and modeling tools are reviewed, potential pros and cons are discussed, and preliminary conclusions are drawn.

PACS numbers: 29.20.db, 41.60.Ap, 88.40.fh

Keywords: Storage rings and colliders, Synchrotron radiation, Advanced Materials

arXiv:1406.0982v1 [physics.acc-ph] 4 Jun 2014

---

\* petracca@sa.infn.it

† arturo.stabile@sa.infn.it

## I. INTRODUCTION

Molecular gas desorption from the beam-pipe wall due to synchrotron radiation should be properly taken into account in the design of high energy particle accelerators and storage rings. This has been a major (solved) challenge for the Large Hadron Collider; will be even more critical for the HE-LHC, in view of its higher level of synchrotron radiation [1], and will be a *crucial* issue for the successful operation of the proposed electron-positron Higgs factories [2].

In the CERN Large Hadron Collider [3] a copper-coated stainless-steel beam pipe (the *liner*) is kept at  $\approx 20K$  by active Helium cooling, and effectively handles the heat load represented by synchrotron radiation, photoelectrons, and image-charge losses. A large number ( $\sim 10^2 m^{-1}$ ) of tiny slots are drilled in the liner wall (see Figure 1) in order to maintain the desorbed gas densities below a critical level (e.g.,  $\sim 10^{15} molecules/m^3$  for  $H_2$ ) by allowing desorbed gas to be continuously cryopumped toward the stainless steel cold bore (co-axial to the liner) of the superconducting magnets, which is kept at  $1.9K$  by superfluid Helium. Above such critical density levels, nuclear scattering in the residual gas would limit the beam luminosity lifetime, eventually originate high energy protons which may cause thermal runaway, and ultimately cause quenching of the superconducting magnets.

The size, geometry, placement and density of the pumping slots affect the beam dynamics

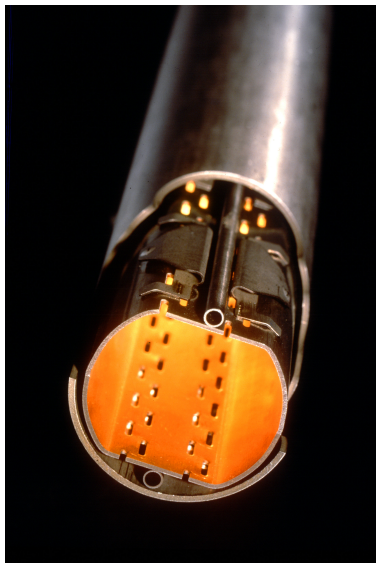


FIG. 1: *The LHC slotted copper-plated beam pipe and stainless steel cold bore.*

and stability in a way which is synthetically described by the longitudinal and transverse beam coupling impedances [4]. The slot geometry and placement should be further chosen so as to minimize the effect of trapped (cut-off) modes, and to prevent the possible coherent buildup of radiation in the TEM waveguide limited by (the outer surface of) the pipe and the cold bore [5].

Open-cell conducting foams could be interesting candidate materials to help fulfilling the above general requirements in beam liner design. In addition, the surface roughness of conducting foams may help reducing the effective secondary-emission yield (SEY) [6], thus alleviating the electron-cloud build-up phenomenon [7], and related instabilities [8]. In this paper we present a brief review of open cell conducting foams properties and modeling tools, and discuss at a very preliminary level the pros and cons of their possible use in high synchrotron radiation accelerator beam liners.

## II. OPEN CELL METAL FOAMS

Open cell metal foams (OCMF) can be produced by vapor (or electro) deposition of metal on an open cell polymer template, followed by polymer burn-off, and a final sintering step to densify the ligaments. Alternatively, they can be synthesised by infiltration/casting of molten metal into a solid mould, consisting of packed (non-permeable) templates of the foam pores, followed by burn-out and removal of the mould [9]. Both processes result into highly gas-permeable *reticular* materials, where only a 3D web of thin conducting ligaments survives. The typical structure of OCMFs is displayed in Figure 2. The key structural

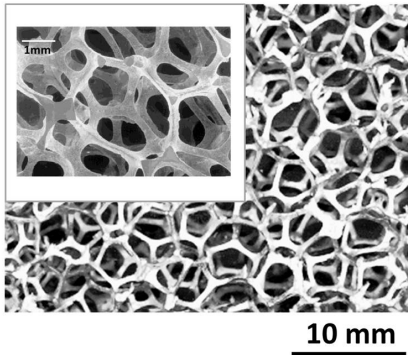


FIG. 2: *A typical open cell metal foam, at two different viewing scales.*

parameters of OCMF are the "pore" size, and the porosity (volume fraction of pores). Pore sizes in the range from  $10^{-4}$  to  $10^{-3}$  *m* and porosities in the range 0.7 - 0.99 are typical. These two parameters determine the gas-permeability of the material, and, together with the electrical properties of the metal matrix, its electrical characteristics. OCMF have remarkable structural properties (low density and weight, high (tensile and shear)-strength to weight ratio, nearly isotropic load response, low coefficient of thermal expansion), as summarized in Table I, which qualified them among the most interesting new materials for aerospace applications. Aluminum and Copper OCMF are presently available off-the-shelf

	Units	<i>Al</i>	<i>Cu</i>
Compressive Strength	[ <i>MPa</i> ]	2.5	0.9
Tensile Strength	[ <i>MPa</i> ]	1.2	6.9
Shear Strength	[ <i>MPa</i> ]	1.3	1.3
Elastic Modulus (Compr.)	[ <i>MPa</i> ]	$1 \cdot 10^2$	$7.3 \cdot 10^2$
Elastic Modulus (Tens.)	[ <i>MPa</i> ]	$1 \cdot 10^2$	$1 \cdot 10^2$
Shear Modulus	[ <i>MPa</i> ]	$2 \cdot 10^2$	$2.8 \cdot 10^2$
Specific Heat	[ <i>J/g<sup>0</sup>C</i> ]	0.89	0.38
Bulk Thermal Cond.	[ <i>W/m<sup>0</sup>C</i> ]	5.8	10.1
Thermal Expansion Coeff.	[ <i>1/<sup>0</sup>C</i> ]	$2.4 \cdot 10^{-5}$	$1.7 \cdot 10^{-5}$
Bulk Resistivity	[ <i>ohm/m</i> ]	$7.2 \cdot 10^{-7}$	$6.5 \cdot 10^{-7}$
Melting Point	[ <sup>0</sup> <i>C</i> ]	660	1100

TABLE I: *Structural properties of Al and Cu open cell metal foams from [10].*

from several Manufacturers worldwide, and are relatively cheap. They can be coated, with Silver, Titanium or Platinum, for special purpose applications. Steel and Brass foams, as well as Silver, Nickel, Cobalt, Rhodium, Titanium or Beryllium foams have been also produced.

The Weaire-Phelan (WP) space-filling honeycombs are credited to provide the *natural* (i.e., Plateau's minimal surface principle compliant) model of OCMF with equal-sized (but possibly unequal-shaped) pores [11]. The WP unit cell consists of a certain arrangement of (irregular) polyhedra, namely two pentagonal-face dodecahedra (with tetrahedral symmetry

$T_h$ ), and six tetrakaidcahedra (with antiprismatic symmetry  $D_{2d}$ ) featuring two hexagonal and twelve pentagonal faces [11]. A computer generated WP honeycomb is displayed in Figure 3, and its visual similarity to Figure 2 is apparent.

A powerful open-source cross-platform software project for 3D morphological characterization and modeling of cellular materials, including OCMF, is under development [12].

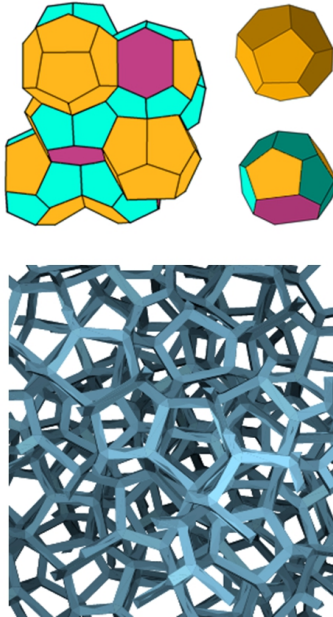


FIG. 3: *The Wearie-Phelan honeycomb cell (top left), its constituent polyhedra (top right), and a numerically simulated reticulated foam thereof (bottom).*

### A. Electrical Properties of Conducting Foams

Electromagnetic modeling of OCMFs has been thoroughly investigated during the last decade. A numerical approach based on Weiland finite integration technique (FIT, [13]) has been proposed by Zhang et al. [14] to compute the (frequency, thickness and angle of incidence dependent) reflection coefficient of *SiC* foam, and optimize its design. The main limitation of Zhang’s analysis is in the use of a simple body-centered-cubic unit-cell foam model, for easiest numerical implementation. The FIT scheme, however may accommodate more complicated and realistic foam-cell geometries, including in principle the WP one. In the quasi-static limit  $\lambda \rightarrow 0$ , the conductivity of OCMFs can be computed using ef-

fective medium theory (EMT), for which several formulations exist (see, e.g., [15],[16] for a review). These include: i) the self-consistent approach [17], credited to Bruggemann, where inclusions are thought of as being embedded in the (actual) effective medium; ii) the differential scheme, whereby inhomogeneities are *incrementally* added to the composite<sup>1</sup>, until the final concentration is reached, so that at each step the inclusions do not interact and do not modify the field computed at the previous step [18]; iii) the effective-field methods, whereby interaction among the inclusions is described in terms of an effective field acting on each inclusion, accounting for the presence of the others. Two main versions of this method exist, credited to Mori-Tanaka [19] and Levin-Kanaun [20], differing in the way the effective field is computed (average over the matrix only, or average over the matrix *and* the inclusions, respectively).

The self-consistent approach yields

$$\sigma_{eff} = \sigma_0(1 - p\nu), \quad (1)$$

where  $\sigma_0$  is the bulk metal conductivity,  $p$  is the porosity (volume fraction of the vacuum bubbles), and  $\nu$  is a morphology-dependent factor. The differential approach yields

$$\sigma_{eff} = \sigma_0(1 - p)^\nu, \quad (2)$$

while the Mori-Tanaka/Levin-Kanaun approaches yield

$$\sigma_{eff} = \sigma_0 / \left(1 + \frac{\nu p}{1 - p}\right). \quad (3)$$

All equations (1)-(3) merge, as expected, in the  $p \rightarrow 0$  limit. The above models are synthetically compared to measured values of the static conductivity in Figure 4, for Aluminum foams. For Aluminum foams, all these models predict *larger* conductivity than observed in measurements<sup>2</sup>. This has been attributed to significant oxide formation on the solid web [22]. Equation (2) agrees in form with predictions based on percolation theory [23] - although strictly speaking there is no threshold here beyond which the conducting component disconnects.

---

<sup>1</sup> In this approach, the total concentration of inhomogeneities does *not* coincide with the volume fraction  $p$ , because at each step new inclusions may be placed where old inclusions have already been set.

<sup>2</sup> It should be noted that open and closed cell metal foams behave similarly in terms of electrical conductivity, while being markedly different as regards thermal conductivity, due to the different role of convective flow.

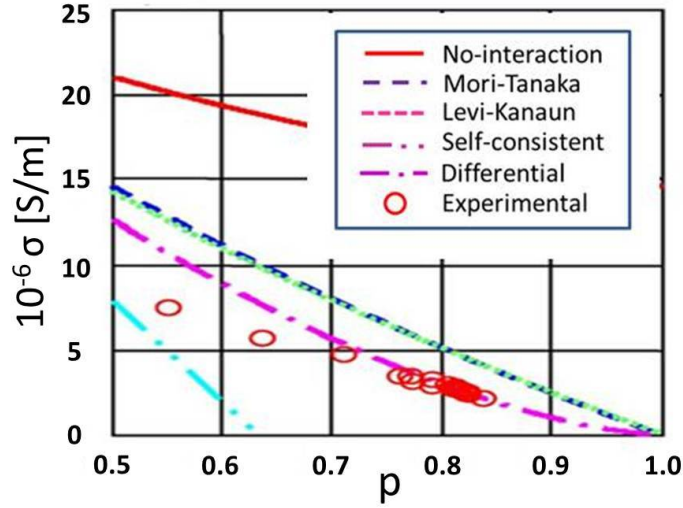


FIG. 4: *Static conductivity vs porosity for Aluminum based foams from different EMT models. Measured values are also shown (adapted from [21]).*

Measurements of the microwave electromagnetic shielding efficiency of OCMF panels [24] indicate that a simple Drude model

$$\sigma(\omega) = \frac{\omega_p^2 \epsilon_0}{i\omega + \nu} \quad (4)$$

provides a good description of the frequency-dependent conductance of metallic foams. Typically, the relevant plasma and collision frequencies,  $\omega_p$  and  $\nu$  are of the order of a few tens of GHz and a few tens of KHz, respectively. These are notably much smaller<sup>3</sup> than their

<sup>3</sup> In the light of the well known formula

$$\omega_p^2 = \frac{N_e q^2}{m_e \epsilon_0},$$

this can be explained as due to a reduction of the electron density  $N_e$ , roughly by a factor  $(1 - p)$ ,  $p$  being the porosity and a parallel (large) increase of the effective electron mass. Pendry et al. have shown that the effective mass of an electron in a thin-conducting-wire lattice or web is essentially set by its electromagnetic momentum, yielding [25]

$$\omega_p^2 \sim \frac{c^2}{D^2 \log(D/d)},$$

where  $d$  and  $D$  are the typical conducting-ligament and pore diameters, respectively, and

$$\nu \sim \frac{\epsilon_0 \omega_p^2}{\pi \sigma_0} \left( \frac{D}{d} \right)^2.$$

solid metal counterparts (typically in the *PHz* and *GHz* range, respectively [26]).

### 1. OCMF Impedance and Skin Depth

Throughout a typical beam current frequency spectrum, OCMF and bulk metals behave quite differently<sup>4</sup>. In bulk metals,  $\omega \ll \nu \ll \omega_p$  so that the characteristic impedance  $Z_m$  and (complex) propagation constant  $\tilde{k}_m$  can be written

$$Z_m \sim \frac{1+i}{\sqrt{2}} \left( \frac{\omega\nu}{\omega_p^2} \right)^{1/2} Z_0, \quad \tilde{k}_m \sim \frac{1-i}{\sqrt{2}} k_0(\omega_p) \sqrt{\frac{\omega}{\nu}} \quad (5)$$

$Z_0$  and  $k_0(\omega) = \omega/c$  being the vacuum characteristic impedance and propagation constant, respectively. It is seen that in metallic conductors, both  $Z_m$  and  $\tilde{k}_m$  are  $\propto \omega^{1/2}$ .

In OCMFs, on the other hand,  $\nu \ll \omega \ll \omega_p$  throughout the beam current spectrum, so that the material exhibits a *plasmonic* behavior. The OCMF wall (characteristic) impedance  $Z_f$  and (complex) propagation constant  $\tilde{k}_f$  are thus given (to lowest order in the small quantities  $\nu/\omega$  and  $\omega/\omega_p$ ) by

$$Z_f \sim Z_0 \left( \frac{\nu}{2\omega_p} + i \frac{\omega}{\omega_p} \right), \quad \tilde{k}_f \sim k_0(\omega_p) \left( \frac{\nu}{2\omega} - i \right) \quad (6)$$

Hence, the OCMF characteristic resistance  $R_f = \text{Re}[Z_f]$  and skin depth  $\delta_f$  are both *frequency independent*, and, e.g., for the case of high-grade ( $\rho \approx 5.510^{-10}$  ohm cm<sup>-1</sup> at 20K) Copper foam with  $p = 0.9$ , both fairly small:

$$R_f \sim \frac{Z_0}{2} \frac{\nu}{\omega_p} \approx 1.4 \cdot 10^{-5} \text{ ohm}, \quad \delta_f \sim \frac{c}{\omega_p} \approx 6 \cdot 10^{-4} \text{ m}. \quad (7)$$

The OCMF characteristic reactance

$$X_f = \text{Im}[Z_f] \sim i Z_0 \frac{\omega}{\omega_p} \quad (8)$$

on the other hand, is large compared to that of bulk metal, and grows *linearly* with  $\omega$ . For the case, e.g., of high-grade Copper foam with  $p = 0.9$ ,  $X_f \approx 0.5$  ohm at 10<sup>4</sup>Hz.

---

<sup>4</sup> The typical power spectrum of a bunched beam in a ring collider consists of lines at integer multiples of  $f_0 = c/\delta_b$ ,  $\delta_b$  being the bunch spacing, with an envelope approximately  $\propto \cos^2$ . In the LHC the -20 dB bandwidth is  $\sim 1$  GHz, roughly 10<sup>5</sup> times the circulation frequency  $\omega_R$ , and 10<sup>-1</sup> times the cut-off frequency of the lowest waveguide mode of the beam pipe [27].



## B. Superconducting Foams

At the operating temperature of the LHC liner ( $\sim 20^{\circ}K$ ), both Aluminum and Copper exhibit a fairly large conductivity ( $\sim 10^7 \text{ ohm}^{-1}\text{cm}^{-1}$ ), but neither of them is superconducting.

Superconducting OCMFs have been discussed in [28]. Foamed *ceramic* superconductors (in particular, YBCOs) with critical temperature well above  $20K$  (HTS), have also been already manufactured [29]. These materials may likely exhibit a very low SEY.

Besides being technologically appealing, HTS foams are conceptually interesting materials, where a percolating electric current co-exists with a percolating magnetic flux [30]. A substantial body of experimental results on the electrical properties of thin-film HTS is available [31], and these are reasonably well accounted for [32] by a simple two-fluid Drude model [33]. However, the electrical properties of *foamed* HTS have been investigated sofar, to the best of our knowledge mostly at very low frequencies [34].

## III. METAL FOAM VS PERFORATED METAL PATCHED PIPES

In this section we shall attempt to draw a comparison between beam pipes using perforated-metal patches for outgassing vs pipes using OCMF patches, in terms of the relevant vacuum and beam-coupling impedance features .

### A. Vacuum Issues

The vacuum dynamics for each molecular species which may be desorbed from the wall by synchrotron radiation can be described by the following set of (coupled) rate equations [35]:

$$\begin{cases} V \frac{dn}{dt} = q - an + b\Theta \\ F \frac{d\Theta}{dt} = cn - b\Theta \end{cases} . \quad (9)$$

Here  $n [m^{-3}]$  and  $\Theta [m^{-2}]$  are the volume and surface densities of desorbed particles, respectively, and  $V$  and  $F$  represent the volume and wall-area of the liner per unit length, respectively.

The first term on the r.h.s. of the first rate equation represents the number of molecules desorbed by synchrotron radiation per unit length and time, and is given by

$$q = \eta \dot{\Gamma}, \quad (10)$$

where  $\eta$  is the desorption yield (number of desorbed molecules per incident photon) and  $\dot{\Gamma}$  is the specific photon flux (number of photons hitting the wall per unit length and time). The second term represents the number of molecules which are removed per unit time and unit length by either sticking to the wall, or escaping through the pumping holes/slots. The  $a$  coefficient in (9) can be accordingly written

$$a = \frac{\langle v \rangle}{4} (s + f) F, \quad (11)$$

where  $\langle v \rangle \approx (8kT/\pi m)^{1/2}$  is the average molecular speed,  $m$  being the molecular mass,  $k$  the Boltzmann constant and  $T$  the absolute temperature,  $\langle v \rangle/4$  is the average number of collisions of a single molecule per unit time and unit wall surface,  $s$  is the sticking probability, and  $f$  is the escape probability. The third term accounts for thermal or radiation induced re-cycling of molecules sticking at the walls. The  $b$  coefficient in (9) can be accordingly written

$$b = \kappa \dot{\Gamma} + F \nu_o \exp(-W/kT). \quad (12)$$

Here the first term accounts for radiation induced recycling, described by the coefficient  $\kappa [m^2]$ , while the second term describes thermally-activated recycling,  $\nu_o$  being a typical molecular vibrational frequency, and  $W$  a typical activation energy.

The  $b\Theta$  term appears with reversed sign on the r.h.s. of the second rate equation, where it represents the number of molecules *de-sticking* from the wall surface per unit time and unit length. The first term on the r.h.s. of this equation represents the number of molecules sticking to the wall, per unit time and unit length, whence (compare with eq. (11))

$$c = \frac{\langle v \rangle}{4} s F. \quad (13)$$

At equilibrium,  $\dot{n} = \dot{\Theta} = 0$ , and the rate equations yield:

$$\left\{ \begin{array}{l} n_{eq} = \frac{4\eta \dot{\Gamma}}{\langle v \rangle f F} \\ \Theta_{eq} = \frac{s}{f} \frac{\eta \dot{\Gamma}}{\kappa \dot{\Gamma} + F \nu_o \exp(-W/kT)} \end{array} \right. \quad (14)$$

Typical values (for LHC) of the parameters in (14) are collected in Table II below [35]. The equilibrium molecular densities in (14) should not exceed some *critical* values for safe

$V$	Liner volume (per unit length)	$1.3 \cdot 10^{-3} \text{ m}^3/m$
$F$	Liner surface (per unit length)	$0.14 \text{ m}^2/m$
$\eta$	Desorption yield	$5 \cdot 10^{-4}$
$\dot{\Gamma}$	Photon flux (200mA beam)	$3.14 \cdot 10^{16} \text{ s}^{-1}m^{-1}$
$s$	Sticking probability	0.6
$\kappa$	Recycling coefficient	$5 \cdot 10^{-21} \text{ m}^2$
$\nu_0$	Vibrational frequency	$10^{13} \text{ s}^{-1}$
$W$	Activation energy	$0.035 \text{ eV/molecule}$

TABLE II: Typical values of the parameters in (14) from [35].

operation [35].

### 1. Liner with Perforated Metal Patches

For a liner wall with vanishing thickness the molecular escape probability  $f$  in (11) and (14) will be given by the holey fraction  $\xi_h$  of the total wall surface. The desorption yield  $\eta$  and the sticking probability  $s$  will likewise differ from those of solid metal by a factor  $(1 - \xi_h)$ .

For a thick perforated wall, the escape probability will be  $f = \chi\xi_h$  where the factor  $\chi < 1$  (named after Clausing), takes into account the possibility that molecules may stick at the hole *internal* surface rather than escaping outside [36].

If only a fraction  $\xi_p$  of the liner surface is covered by perforated patches, the liner escape probability will be  $f = \xi_p\chi\xi_h$ .

In the LHC the pumping holes are thin slots parallel to the pipe axis [37]. The slots are confined to four narrow ( $\approx 9\text{mm}$  wide) strip-shaped patches, running parallel to the pipe axis, as seen in Figure 1. The escape probability of an LHC-like slotted patch (strip) is displayed in the left panel of Figure 5. Stiffness requirements set a lower limit to the axial ( $s_L$ ) and transverse ( $s_T$ ) slot spacings at roughly twice the slot width  $w$ . In figure 5 we assume  $s_T = 2w$  and plot the escape probability vs. the scaled longitudinal slot separation

$s_L/2w$ , for three typical values of the slots height-to-width ratio  $h/w$ . The wall thickness  $\Delta$  is assumed as equal to  $w$ , yielding a Clausing factor  $\chi \approx 0.68$  [38].

In the LHC the slotted strips represent roughly one half of the liner surface. The slots are  $\approx 8\text{mm}$  long, on average, and  $\approx 1.5\text{mm}$  wide, with  $s_L \approx s_T \approx 3\text{mm}$ . The holey fraction of the total liner surface is roughly 5%, and the escape probability is  $\approx 3.5\%$ .

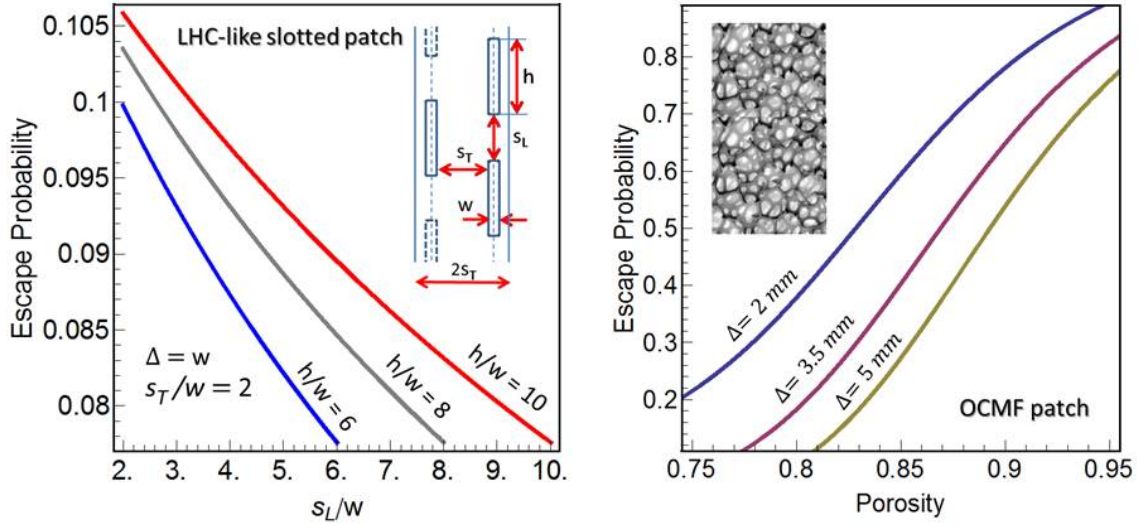


FIG. 5: *Left panel: escape probabilities for LHC-like slotted patches. Right panel: escape probability for OCMF patches.*

## 2. Liner with OCMF Patches

Gas permeability of OCMFs in the molecular flow regime is described by Knudsen diffusivity [36]. The dependence of this latter on foam porosity was fitted numerically in [39] and [40], using computer simulations of molecular diffusion based on tomographic data of actual OCMF specimens. An exponential blow up of Knudsen diffusivity  $D_K$  was observed, above

some porosity threshold, possibly due to the creation of long-range molecular pathways. From Knudsen diffusivity the escape probability of OCMF patches can be readily obtained, using Fick's (diffusion) law, and is displayed in Figure 5 (right panel) as a function of porosity, for different values of the OCMF wall thickness  $\Delta$ .

It is seen from Figure 5 that typical OCMF patches, e.g., with  $p = 0.9$ , feature fairly larger escape probabilities, compared to slotted patches.

OCMF walls are also expected to provide better EM shielding compared to slotted ones. Hence, gas molecules sticking inside the foam pores will be less exposed to recycling, resulting into possibly smaller values of the recycling factor  $\kappa$  in (12) and (14).

## B. Beam Coupling Impedance and Parasitic Losses

Beam coupling impedances provide a synthetic description of the electromagnetic beam-pipe interaction. Here, for the sake of brevity, we shall confine our discussion to the longitudinal impedance. The absolute value and the imaginary part of this latter are inversely proportional to the threshold currents for (single-bunch) microwave instability and Landau damping suppression, respectively, and hence quite relevant to beam stability [4], while the real part determines the parasitic loss (energy lost by the beam per unit pipe length), via [4]

$$\Delta\mathcal{E} = \frac{1}{2\pi} \int_{-\infty}^{+\infty} |I(\omega)|^2 \Re [\bar{Z}^{\parallel}(\omega)] d\omega, \quad (15)$$

where  $I(\omega)$  and  $Z^{\parallel}(\omega)$  are the beam-current spectrum and longitudinal impedance per unit length, respectively.

The following relationship exists (to 1st order in the wall impedance) between the longitudinal impedance per unit length  $\bar{Z}_{\parallel}$  of a patched-wall beam liner and the (known) longitudinal impedance per unit length  $\bar{Z}_{\parallel}^{(0)}$  of the same pipe with a perfectly conducting wall [41]

$$\bar{Z}_{\parallel} = \bar{Z}_{\parallel}^{(0)} + \frac{\epsilon_0 Y_0}{c\Lambda^2} \oint_{\partial S} Z_w(s) |E_{0n}(s)|^2 ds, \quad (16)$$

where  $Z_w$  is the (local) Leontóvich impedance [42] of the patched wall,  $\partial S$  is the pipe cross-section contour,  $Y_0 = (\epsilon_0/\mu_0)^{1/2}$  the vacuum admittance,  $\Lambda$  the beam linear charge density, and  $E_n^{(0)}$  the (known) field component normal to the pipe wall in the perfectly conducting

pipe<sup>5</sup>. According to (16), perforated/slotted or OCMF patches placed where the normal field component  $E_n^{(0)}$  is *minimum* will have minimum impact on the longitudinal impedance. Hence, a circular beam liner, featuring a *uniform* field along  $\partial S$ , represents a worst case, where the longitudinal (and transverse) beam coupling impedances is simply proportional to the average of the wall impedance, assumed as piecewise constant

$$\langle Z_{wall} \rangle = \sum_i \xi_i Z_{wall}^{(i)} \quad (17)$$

$\xi_i$  being the surface fraction covered by patches with wall impedance  $Z_{wall}^{(i)}$ .

### *Impedance of Perforated Patch*

The effective wall impedance of a perforated patch can be computed under the Bethe approximation where the holes/slots are (much) smaller than the shortest wavelength in the beam spectrum, yielding [43], [44]

$$Z_s^{(0)} = \imath Z_0 \left( \frac{\omega}{c} \right) \alpha_{tot}^{(i)} n_\sigma \quad (18)$$

$Z_0 = (\mu_0/\epsilon_0)^{1/2}$  being the vacuum characteristic impedance,  $\alpha_{tot}^{(i)}$  the total internal polarizability of the holes/slots, and  $n_\sigma$  their surface density.

In [45] the more general case, relevant for the LHC, of a circular perforated liner with inner radius  $a$  and thickness  $\Delta$  surrounded by a circular co-axial lossy tube (the cold bore) with radius  $b$  was investigated. It was found that the liner wall impedance can still be cast in the form of eq. (18), after the formal substitution

$$\alpha^{(i)} \longrightarrow \alpha^{(i)} + F\alpha^{(e)}, \quad (19)$$

where the superfix  $(e)$  identifies the total *external* polarizability of the holes/slots in wall with thickness  $\Delta$ , and [44], [45]

$$F = -\frac{\alpha^{(e)}}{\alpha^{(i)}} \left[ 1 + \imath \left( 1 + \frac{b}{a+\Delta} \right) \frac{Z_{cb}}{Z_h^{(0)}} \right]^{-1}, \quad (20)$$

$Z_{cb}$  being the cold bore wall impedance <sup>6</sup>. The wall reactance is negligibly affected by the presence of the external tube, which produces a small resistive component, accounting for

<sup>5</sup> A similar formula exists for the (dyadic) transverse impedance [41].

<sup>6</sup> In this formula  $Z_{cb}$  is the impedance of both the the cold bore and outer beam-liner walls.

radiation leakage through the slots.

We use the following formulas from for thin axial slots from [46] :

$$\alpha_{tot}^{(0)} = w^3(0.1334 - 0.005w/h), \quad \alpha_{tot}^{(i)} = (8/\pi^2)\alpha_{tot}^{(0)}, \quad \alpha_{tot}^{(e)} = \exp(-\pi\Delta/w)\alpha_{tot}^{(0)}, \quad (21)$$

where  $\alpha_{tot}^{(0)}$  is the total polarizability of a slot in a vanishingly thin wall, and all other symbols are defined in Figure 5.

### *Impedance of OCMF Patch*

A straightforward solution, which is not included for brevity, of the electromagnetic boundary value problem for a (relativistic, vanishingly thin) axial beam in a circular conducting foam liner, with radius  $a$  and thickness  $\Delta$  surrounded by a co-axial (infinitely thick) conducting circular tube (the cold bore) with radius  $b > a + \Delta$ , shows that if  $\Delta$  exceeds a few skin depths  $\delta_f$  across the whole beam current spectrum, which is certainly the case here, as seen from eq. 7, the Leontóvich impedance of the OCMF liner wall is fairly well approximated by the intrinsic impedance of the OCMF, viz., (compare w. eq (6)

$$Z_f = Z_0 \left( \frac{\nu}{2\omega_p} + i \frac{\omega}{\omega_p} \right). \quad (22)$$

The surface *roughness* of the foam also contributes to the OCMF wall impedance. The order of magnitude of this contribution can be estimated from [47]

$$Z_f^{(rough)} \approx i \sqrt{\frac{\pi}{32}} Z_0 \left( \frac{h}{L} \right) \frac{\omega}{c} h, \quad (23)$$

$h$  and  $L$  being the r.m.s. height and correlation length of the surface roughness, respectively.

### *Impedance Budget*

For illustrative purposes, the numerical values of the real and imaginary components of the relevant wall impedances, normalized to the mode number (i.e., multiplied by the  $(\omega_R/\omega)$  factor), have been collected in Table III. Here we assume high-grade Copper ( $\rho \approx 5.510^{-10}$  ohm cm<sup>-1</sup> at 20K) for the solid, slotted, and foam-matrix metal.

The numbers in Table III for the slotted-patch are obtained for the slot geometry depicted in Figure 5, with  $w = \Delta = 1.5\text{mm}$ ,  $h = 10w$  and  $s_T = s_L = 2w$ , for which  $\xi_h \approx 0.14$ , and the escape probability reaches its the fiducial upper limit  $f \approx 0.1$ .

The numbers for the foamed patch are obtained assuming a typical pore diameter  $\sim 1\text{ mm}$ , and a typical ligament size  $\sim 0.1\text{ mm}$ , yielding  $\omega_p \approx 7.93 \cdot 10^{10}\text{ rad sec}^{-1}$  and  $\nu \approx 3.66 \cdot 10^4\text{ Hz}$  in the Drude model of Section II A 1, consistent with typical measured values of the static conductance of open-cell Copper foams. We assume a typical r.m.s. roughness scale  $h \approx .125\text{ mm}$  and a correlation length  $L \approx 0.25\text{ mm}$ .

	Solid Copper Patch	OCMF Patch	OCMF Roughness	Slotted Patch (Perfect Conductor)
$(\omega_R/\omega)R_{wall}$ , [ohm]	$4.9 \cdot 10^{-6}\sqrt{\omega_R/\omega}$	$1.4 \cdot 10^{-5}(\omega_R/\omega)$	0	$1.0 \cdot 10^{-13}\sqrt{\omega/\omega_R}$
$(\omega_R/\omega)X_{wall}$ , [ohm]	$4.9 \cdot 10^{-6}\sqrt{\omega_R/\omega}$	$5.5 \cdot 10^{-5}$	$5.5 \cdot 10^{-6}$	$3.1 \cdot 10^{-7}$

TABLE III: *Summary of Leontóvich impedances. High-grade Copper with  $\rho \approx 5.510^{-10}\text{ ohm cm}^{-1}$  at 20K. OCMF with 1mm pores and 0.1mm ligaments. Slots in a perfectly conducting wall as in Figure 5, with  $w = \Delta = 1.5\text{mm}$ ,  $h = 10w$  and  $s_T = s_L = 2w$ .*

As seen from Table III, the Copper wall resistance is larger than that of the OCMF up to  $\omega = 10^5\omega_R$ . On the other hand, as anticipated in Section II A 1, the OCMF wall reactance is relatively large, and exceeds significantly that of a perfectly conducting slotted wall as well as that of solid Copper.

However, as seen from Figure 5, a typical OCMF wall pumping capacity (escape probability) is several times larger than that of the "best" slotted wall. Thus, to obtain the same pumping capacity, the patched beam-liner surface needed in the OCMF case is only a small fraction of that for the slotted case. This makes easier to place the OCMF patches where the (unperturbed) field in eq. (16) is minimum, so as to minimize their impact on the beam coupling impedance.



### C. Secondary Emission Yield

Perforations reduce the secondary emission yield (SEY) of a metal wall by a factor roughly proportional to the solid fraction of the surface [6].

The SEY of metals is strongly reduced by surface roughening, obtained, e.g., by powder blasting [8]. For the special case of periodic rectangular grooves etched on a flat metal surface, the SEY dependence on the groove depth-to-spacing and width-to-thickness ratios has been investigated, indicating that larger ratios yield a smaller SEY [48].

Carbon coating also reduces SEY effectively [49], at the expense of some increase in wall resistance.

It is reasonable to expect that OCMFs may exhibit a much lower SEY compared to solid metals in view of their random-like surface roughness. The SEY of an OCMF wall will depend on the effective roughness of its surface, which is a function of the foam porosity and average pore size. OCMF surface roughness, however, should be kept small enough, to prevent the blow up of wall reactance. No measurements of the SEY of OCMFs are available yet, to the best of our knowledge, but should be straightforward [50].

## IV. CONCLUSIONS

On the basis of the above discussion, some tentative conclusions can be drawn about the possible use of OCMF materials in the beam liners of high synchrotron radiation accelerators. The outgassing capabilities of OCMF patches can be better by a factor  $\sim 10$  compared to the "best" slotted patches, and would accordingly allow to boost the molecular escape probability of beam pipes by roughly one order of magnitude, compared to present designs, while keeping the patched fraction of the beam-liner surface unchanged.

The mechanical-structural properties of conducting foams should also be adequate to resist to eddy-current induced stresses, in view of their very morphology.

A low SEY is also expected, due to OCMF surface roughness, even though no experimental results are available yet.

The OCMF surface resistance is very low, and almost frequency independent. On the other hand, the (inductive) wall reactance of an OCMF patch is larger by roughly one order of magnitude compared to that of a perforated wall with comparable escape probability. This

drawback could be mitigated by clever placement of the OCMF patches, and/or appropriate reactive loading of the (solid portion of) the pipe wall.

In order to translate the above hints into effective design criteria, further modeling effort and substantial experimental work are in order. Measurement of the complex surface impedance and SEY of metal foams are now underway [51].

We believe that such an effort is worth being pursued, and that the available modeling tools and technologies provide a good starting point for its successful implementation.

### Acknowledgements

This work has been sponsored in part by the Italian Institute for Nuclear Physics (INFN) under the IMCA grant. Stimulating discussions with F. Zimmermann and G. Rumolo (CERN) are gratefully acknowledged.

- 
- [1] A. Valishev, "Synchrotron Radiation Damping, Intrabeam Scattering and Beam-Beam Simulations for HE-LHC," arXiv:1108.1644v1 [physics.acc-ph] (2011).
  - [2] A. Blondel et al., "LEP3: A High Luminosity e+e- Collider to Study the Higgs Boson," arXiv:1208.0504v2 [physics.acc-ph] (2012).
  - [3] - "The Large Hadron Collider Conceptual Design," CERN Rept. AC/95-05 (1995).
  - [4] B.W. Zotter and S.A. Kheifets, "*Impedances and Wakes in High Energy Particle Accelerators*," World Scientific, Singapore (1998).
  - [5] S. Heifets and A. Mikhailichenko, "Coherent Synchrotron Radiation in Multiply Connected Vacuum Chamber," SLAC Pub. 8428 (2000).
  - [6] I. Montero et al., "Lowering SEY by Rough Surfaces," Proc. CERN Anti e-Cloud Coating AEC '09, paper #29.
  - [7] F. Zimmermann, "Review of Single Bunch Instabilities Driven by an Electron Cloud," PRST-AB 7 (2004) 124801.
  - [8] K.C. Harkay, "Observation and Modeling of Electron Cloud Instability" Proc. EPAC '06, Edinburgh UK, paper id. WEXFI02 (2006).
  - [9] J. Banhart and N.A. Fleck, "*Cellular Metals and Metal Foaming Technology*," MIT Press,

- Boston (2003).
- [10] [www.ergaerospace.com](http://www.ergaerospace.com)
- [11] D. Weaire and R. Phelan, "A Counter-Example to Kelvin's Conjecture on Minimal Surfaces," *Phil. Mag. Lett.* **69** (1994) 107.
- [12] [www.imorph.sourceforge.net](http://www.imorph.sourceforge.net)
- [13] T. Weiland, "A Discretization Method for the Solution of Maxwells Equations for Six-Component Felds," *AEU Int. J. Electr.* **C31** (1977) 116.
- [14] H. Zhang et al., "Numerical Predictions for Radar Absorbing Silicon Carbide Foams Using a Fnite Integration Technique with a Perfect Boundary Approximation," *Smart Mater. Struct.* **15** (2006) 759.
- [15] F.G. Cuevas et al., "Electrical Conductivity and Porosity Relationship in Metal Foams," *J. Porous. Mater.* **16** (2008) 675.
- [16] R. Goodall, L. Weber and A. Mortensen, "The Electrical Conductivity of Microcellular Metals," *J. Appl. Phys.*, 100 (2006) 044912.
- [17] D.A.G. Bruggemann, "Berechnung Verschiedener Physikalischer Konstanten von Heterogenen Substanzen," *Ann. Phys.* **24** (1935) 636.
- [18] R. McLaughlin, "A Study of the Differential Scheme for Composite Materials," *Int. J. Eng. Sci.* **5** (1977) 237.
- [19] Y. Qui and G.J. Weng, "On the Application of MoriTanaka's Theory Involving Transversely Isotropic Spheroidal Inclusions," *Int. J. Eng. Sci.* **28** (1990) 1121.
- [20] S.K. Kanaun, "Dielectric Properties of Matrix Composite Materials with High Volume Concentration of Inclusions (Effective Field Approach)," *Int. J. Eng. Sci.* **41** (2003) 1287.
- [21] I. Sevostianov, J. Kovacic and F. Simancik, "Elastic and Electric Properties of Closed Cell Aluminum Foams," *Mat. Sci. Eng.* **A420** (2006) 87.
- [22] T. W. Clyne, Thermal and Electrical Conduction in MMCs, in "*Comprehensive Composite Materials*," Elsevier, Amsterdam (2000).
- [23] D. Stauffer and A. Aharony, "*Introduction to percolation Theory*," Taylor and Francis, London (1992).
- [24] G. Monti et al., "New Materials for for Electromagnetic Shielding: metal Foms with Plasma Properties," *Microwave Opt. Technol. Lett.*, **B52** (2010) 1700.
- [25] J.B. Pendry et al. "Low Frequency Plasmons in Thin-Wire Structures," *J. Phys. Cond. Matt.*

- 10** (1998) 4785.
- [26] M.A. Ordal et al., "Optical Properties of the Metals *Al, Co, Cu, Au, Fe, Pb, Ni, Pd, Pt, Ag, Ti* and *W* in the Infrared and Far Infrared," *Appl. Optics* **22** (1983) 1099.
- [27] H. Day et al., paper WEPPR070, Proceedings of IPAC2012 (2012)
- [28] E.S. Reddy and G.J. Schmitz, "Superconducting Foams," *Supercond. Sci. Technol.* **15** (2002) L21.
- [29] E.S. Reddy et al., "Processing of  $Y_2BaCuO_5$  Foams," *Supercond. Sci. Technol.* **16** (2003) 608.
- [30] E. Bartolomé et al., "Critical State in Superconducting Single-Crystalline  $YBa_2Cu_3O_7$  Foams: Local versus Long-Range Currents," *Phys. Rev.* **B 70** (2004) 144514.
- [31] D.N. Basov et al., "Electrodynamics of High- $T_c$  Superconductors," *Rev. Modern Phys* **77** (2005) 721.
- [32] C.A.M. dos Santos et al., "Two Fluid Model for Granular Superconductors," *Phys. Rev.* **B74** (2006) 184526.
- [33] J.H. Ma and I. Wolf, "Modeling the Microwave Properties of Superconductors," *IEEE Trans.MTT-42* (1985) 1053.
- [34] J.G. Noudem, "Magnetic and Transport Properties of  $YBa_2Cu_3O_y$  Superconductor Foams," *Physica* **C390** (2003) 286.
- [35] O. Gröbner, "Overview of the LHC Vacuum System," *Vacuum* **60** (2001) 25.
- [36] W. Steckelmacher, "Knudsen Flow 75 Years on: the Current State of the Art for Flow of Rarefied Gases in Tubes and Systems," *Rep. Progr. Phys.* **49** (1986) 1083.
- [37] O Malyshev, CERN "LHC Vacuum Technical Note 01-06," (2001).
- [38] W. Steckelmacher and K.F. Man, "Molecular Flux Distribution in the Detector Plane of an Effusive Source Molecular Beam Apparatus," *Rev. Sci. Instrum.* **56** (1985) 58 (1985).
- [39] T. Fiedler et al., "Numerical Simulation of Knudsen Diffusion in a Metallic Foam," *Comput. Mat. Sci.*, **50** (2011) 1795.
- [40] T. Fiedler et al., "A Comparative Study of Knudsen Diffusion in Cellular Metals," *Comput. Mat. Sci.*, **50** (2011) 2666.
- [41] S. Petracca, "Reciprocity Theorem for Coupling Impedance Computation in the LHC Liner.," *Particle Accel.* **50** (1995) 211.
- [42] A.M. Dykne and I.M. Kaganova, "The Leontovich Boundary Conditions and Calculation of Effective Impedance of Inhomogeneous Metal," *Opt. Comm.* **206** (2002) 39.

- [43] S.S. Kurennoy, "Coupling Impedance of Pumping Holes," *Particle Accel.* **39** (1992) 1.
- [44] S. Petracca, "Beam Coupling Impedances for Perforated Beam Pipes with General Shape from Impedance Boundary Conditions," *Phys. Rev.* **E60** (1999) 6030.
- [45] R.L. Gluckstern and B.W. Zotter, "Energy loss to Coaxial Vacuum Chambers in LEP and LHC," CERN Rept. SL 96/56 (AP) 1996.
- [46] S. Kurennoy, "Coupling Impedances and Heating due to Slots in the KEK B Factory," KEK-preprint 94-193 (2005).
- [47] K.L.F. Bane and G.V. Stupakov, "Wake of a Rough Beam Wall Surface," SLAC Pub. 8023 (1988).
- [48] M. Pivi et al., "Sharp Reduction of the Secondary Electron Emission Yield from Grooved Surfaces," SLAC Pub. 13020 (2007).
- [49] C.Y. Vallgren et al., "Amorphous carbon coatings for the mitigation of electron cloud in the CERN Super Proton Synchrotron," *Phys. Rev. STAB* **14** (2011) 071001.
- [50] F. Caspers et al., "RF Test Benches for Electron Cloud Studies," Proceedings EPAC '02, Paris, FR, paper id WEPDO031 (2002).
- [51] R. Cimino, S. Petracca and A. Stabile, work in progress.